

Monitoring synchrotron X-ray-induced radiolysis effects on metal (Fe, W) ions in high-temperature aqueous fluids

Robert A. Mayanovic,^{a*} Alan J. Anderson,^b Hingure A. N. Dharmagunawardhane,^a Sakura Pascarelli^c and Giuliana Aquilanti^d

^aDepartment of Physics, Astronomy and Materials Science, Missouri State University, Springfield, MO 65897, USA, ^bDepartment of Earth Sciences, St Francis Xavier University, PO Box 5000, Antigonish, Nova Scotia, Canada B2G 2W5, ^cEuropean Synchrotron Research Facility, Grenoble, France, and ^dSincrotrone Trieste, ss 14, km 163.5, Trieste, I-34149 Basovizza, Italy.
E-mail: robertmayanovic@missouristate.edu

Radiolysis-induced effects on aqueous tungsten ions are observed to form a precipitate within seconds upon exposure to a synchrotron X-ray micro-beam in a $\text{WO}_3 + \text{H}_2\text{O}$ system at 873 K and 200 MPa. *In situ* Fe K-edge energy-dispersive X-ray absorption spectroscopy (ED-XAS) measurements were made on Fe(II)Cl_2 aqueous solutions to 773 K in order to study the kinetics of high-temperature reactions of Fe^{2+} and Fe^{3+} ions with transient radiolysis species. The radiolytic reactions in a fluid sample within a hydrothermal diamond anvil cell result in oxidation of the Fe^{2+} ion at 573 K and reduction of Fe^{3+} at temperatures between 673 and 773 K and of the Fe^{2+} ion at 773 K. The edge-energy drift evident in the ED-XAS data directly reflects the kinetics of reactions resulting in oxidation and/or reduction of the Fe^{2+} and Fe^{3+} ions in the aqueous solutions at high temperatures. The oxidation and reduction trends are found to be highly consistent, making reliable determinations of reaction kinetics possible.

Keywords: energy-dispersive XAS; radiolysis; oxidation/reduction; hydrothermal fluid.

1. Introduction.

Next-generation water-cooled nuclear reactors are expected to operate at higher efficiencies utilizing pure water in the primary cooling loop to temperatures and pressures exceeding the supercritical point (647 K and 22.06 MPa) [see Bouchard (2009) and Boyle *et al.* (2009) and other contributions in those proceedings]. The modifications in the chemistry of water due to radiolysis are expected to play a significant role in the oxidation/corrosion of the components of nuclear reactors utilizing supercritical water cooling (*e.g.* GenIV reactors). Although significant progress has been made in understanding radiation-induced chemistry of water to near and supercritical conditions (Elliot, 1994; Elliot *et al.*, 1996; McCracken *et al.*, 1998; Garrett, 2005), the effects of radiolysis on the physico-chemical properties of solutes in aqueous systems under elevated temperatures and pressures are not well known (Christensen, 2006). Studies of this nature are necessary in order to theoretically model and control water chemistry of supercritical-water-cooled nuclear reactors and thereby limit corrosion principally within the reactor's primary cooling loop.

Ionizing radiation causes radiolysis of water, producing transient species such as H^\bullet , $\bullet\text{OH}$, H^+ , OH^- and hydrated electrons, e_{aq}^- . These species react with each other resulting in the production of H_2O_2 , dissolved H_2 and O_2 , and other by-products. The energy from the ionizing radiation is deposited along spurs where competing mechanisms of diffusion and recombination of transients results in the production of secondary radiolysis species within a 10^{-12} to 10^{-6} s time scale (Draganic & Draganic, 1971; Spinks & Woods, 1990). The transient radiolysis species and their products (principally the radicals) react with solutes thus modifying the chemical properties of aqueous fluids. The production of H_2O_2 and O_2 that results from radiolysis in nuclear power reactors is of concern because these products may persist for days or weeks and may cause considerable oxidation and corrosion of the primary cooling loop components. The metal ions that result from corrosion of steel-based alloy materials, such as Fe^{3+} , Ni^{2+} , Co^{2+} and W^{6+} , are transported in the heated water of the primary cooling loops of nuclear power reactors (Shaw *et al.*, 1991). The dissolved metal ions typically lower the pH and enhance the corrosiveness of the aqueous fluid within the primary cooling loop (Kritzer, 2004). Direct *in situ* measure-

ment of dissolved metal ions near the core or in the primary cooling loop of nuclear reactors, under the extremes of temperature, pressure and radiation, is currently not feasible. As we show below, the use of the hydrothermal diamond anvil cell and synchrotron beamlines allows for *in situ* studies of radiolysis effects due to ionizing radiation on metal ions in aqueous fluids to supercritical conditions.

The advent of focused X-ray beams from high-brilliance third-generation synchrotron sources has resulted in greater incidence of X-ray-radiolysis-induced oxidation or reduction of solutes, making determination of the structure of aqueous complexes or catalytic properties of aqueous species more problematic (Mesu *et al.*, 2006). Conversely, however, radiolysis due to synchrotron radiation combined with the capability for time-resolved measurements offers opportunities for kinetic X-ray studies of radiolysis-induced chemical reactions in aqueous systems under extreme conditions. Whereas the products of water radiolysis remain unchanged with type of ionizing radiation, the amount of linear energy transfer (LET) differs somewhat for neutrons and X-rays. Fast neutron recoil protons deposit LETs in the range 10–70 eV nm⁻¹ (Spinks & Woods, 1990) whereas 10 keV X-rays give an LET of 4.1 eV nm⁻¹ (Ferradini & Jay-Gerin, 2000). Higher LET results in a greater yield of molecular radiolysis products (O₂, H₂ *etc.*) and lower LET results in a larger fraction of radical products (*e.g.* OH, H *etc.*) from radiolysis escaping the spur tracks. Radiolysis effects on iron and copper species due to synchrotron X-ray-induced radiolysis in aqueous fluids, at room- to high-temperature conditions, have been noted by our group in previous experiments (Bassett *et al.*, 2000a; Jayanetti *et al.*, 2001; Mayanovic *et al.*, 1999). Our study of room-temperature Cu(II)Cl₂ aqueous solutions examined the effects of X-ray-radiolysis-induced reduction of copper species leading to formation of copper clusters and nanoparticles (Jayanetti *et al.*, 2001): the rate of reduction of copper species was found to increase with increasing X-ray beam flux. As described in greater detail below, our initial XAS experiments on Fe(II)Cl₂ aqueous solutions revealed that X-ray-radiolysis-induced effects cause oxidation or reduction of iron species depending upon the pressure–temperature (*P–T*) conditions of the fluid. However, the capabilities to carry out a kinetic study of X-ray-induced radiolysis effects on aqueous iron species using synchrotron energy-dispersive X-ray absorption spectroscopy (ED-XAS) have been available only recently. This paper describes a novel use of the ED-XAS technique for an *in situ* kinetic study of the oxidation of Fe²⁺ and reduction of Fe²⁺ and Fe³⁺ ions, resulting from reactions with radiolytic species in subcritical and supercritical aqueous fluids. In addition, we also discuss X-ray-induced radiolysis effects on a sample of WO₃ in water to high temperature and pressure conditions. The aim of this paper is twofold:

- (i) To demonstrate the potential of the ED-XAS technique for *in situ* kinetic studies of X-ray-induced radiolytic effects on solutes in aqueous solutions to high *P–T* conditions.
- (ii) To bring attention to the potential effects of synchrotron X-ray-induced radiolysis on speciation- and structure-related

studies of solutes in aqueous fluids, particularly under high *P–T* conditions.

2. Radiolysis effects on tungsten species in a high-temperature aqueous solution

The use of tungsten in ferritic and martensitic steels has great potential for future nuclear power reactor applications (Klueh, 2004). Similarly, tungsten is envisioned to play an important role in the design of blanket materials for future fusion reactors (Ihli *et al.*, 2008). Provided these materials come in contact with supercritical water, formation of oxide products upon corrosion and oxidation such as WO₃ may help in providing a passivation layer on the inner cladding of primary cooling loop systems, reactor vessel walls, and other nuclear reactor components. In addition, WO₃ has considerable potential for use in supercritical water technology gas sensor applications (Hoel *et al.*, 2004). Although synchrotron XAS measurements have been made on aqueous tungstate solutions to 673 K (Hoffmann *et al.*, 2000), studies of radiolysis-induced effects on tungsten species or on the solubility of WO₃ in aqueous systems under elevated temperatures and pressures are lacking. We had initially intended to make synchrotron structure studies of aqueous tungsten species and solubility studies of WO₃ in aqueous solutions to high *P–T* conditions. Our initial attempt to study WO₃ solubility in aqueous solutions to high *P–T* conditions showed that the chemistry of the aqueous fluid was significantly altered during exposure to the X-ray beam (see §5.1).

3. Radiolysis-induced oxidation and reduction of iron species in a high-temperature aqueous solution

Iron constitutes one of the key contaminants in pressurized and boiling water nuclear reactors (Neeb, 1997) and has been shown to dissociate owing to corrosion from the surface of Hastelloy-C coupons into supercritical water containing less than 100 p.p.b. dissolved oxygen (Guzonas *et al.*, 2009). In addition, ⁵⁹Fe is a significant transition metal radionuclide contributing to radiation in the primary loop of a water-cooled nuclear reactor. The reactions involving aqueous Fe²⁺ and Fe³⁺ ions with transient radiolysis species and radiolytic products (to subcritical temperatures) have been studied widely, primarily because of the use of ferrous sulfate solutions in the Fricke dosimeter (see Matthews, 1982; LaVerne & Pimlott, 1993, and references therein). The only kinetic studies known to the authors of aqueous Fe solutions at elevated *P–T* conditions are of the reactions involving the Fe²⁺ ion and the •OH and •O₂H radicals in aqueous solution using pulse radiolysis by Christensen & Sehested (1981) to 493 K, and by Lundström *et al.* (2004) to 391 K. However, the radiation-induced chemistry, including the kinetics of chemical reactions, of species resulting from radiolysis reacting with Fe²⁺ and Fe³⁺ ions in supercritical aqueous fluids is not well understood.

The reactions involving primary radiolysis species can cause an oxidizing or reducing environment, depending upon the

chemistry, P - T conditions and types of solutes present in the aqueous solution (Buxton, 1987; Garrett, 2005). Fig. 1 shows our Fe K -edge XANES data measured previously from a 0.1 M Fe(II)Cl₂ aqueous solution sample in a hydrothermal diamond anvil cell, in the temperature range from 298 to 773 K (Anderson *et al.*, 2012). The measurements were made using capillary focusing at the B2 bending-magnet beamline of the Cornell High Energy Synchrotron Source (CHESS). The XANES data were measured at different temperatures during heating and cooling of the sample over a three-day and 15 h period [see an illustration of the thermal history of the sample in Fig. 1(c)]. From the shift in the Fe K -edge energy and appearance of the XANES in Fig. 1, it is evident that either oxidation or reduction of iron species occurs, depending upon the P - T conditions and thermal trajectory of the aqueous solution sample. Heating the sample from 298 to 573 K and exposure to the X-ray beam resulted in a shift of the edge to higher energy values accompanied by a change in appearance primarily of the above-edge XANES towards that of the Fe(III)Cl₃ aqueous solution. In contrast, continued heating and X-ray-beam irradiation of the sample at 673 and 773 K resulted in a shift of the Fe K -edge to lower energy values and a change in appearance of the XANES (both below and above the edge) towards that of iron metal. The amount of shift in Fe K -edge energy and change in appearance of the XANES were found to be dependent upon the length of time of exposure of the sample to the X-ray beam. The reduction of iron species occurring during irradiation at 673 and 773 K resulted in the appearance of a black colloidal or fine-grained precipitate. Cooling of the sample under the conditions illustrated in Fig. 1(c) resulted in dissolution of the precipitate back into solution. In addition, cooling the sample and exposure to the X-ray beam resulted in a shift of the Fe K -edge to higher energy values and a change in the appearance of the XANES towards that of Fe(II)Cl₂ aqueous solution. The time-resolved *in situ* ED-XAS analysis described below was needed to

investigate the kinetics of X-ray-beam-induced chemical reactions involving primary radiolysis products and iron species in chloride-bearing aqueous solutions under elevated P - T conditions.

4. Materials and methods

4.1. WO₃ + H₂O system

Single crystals of tungsten trioxide (WO₃) were prepared by placing tungsten(VI) oxide powder of 20 μ m grain size (Aldrich) in a capped Pt crucible and heating in air at 1673 K for 120 min. The crystals produced in the crucible were ≤ 200 μ m in size and were identified as monoclinic WO₃ (space group $P1$) from powder X-ray diffraction data obtained using a PANalytical X'pert PRO diffractometer. A single crystal of WO₃, ~ 40 μ m in diameter, was loaded into the hydrothermal diamond anvil cell (HDAC) with a small amount of deoxygenated water. The sample was placed in a recess in the culet face of the lower diamond anvil, measuring 300 μ m in diameter and 40 μ m in depth, and sealed between the diamond anvils without the use of a gasket (Chou *et al.*, 2008). The sample pressure at a given temperature was estimated from the equation of state of water (Wagner & Pruss, 2002), using the density of water in the HDAC as determined from the temperature of liquid-vapor homogenization. Synchrotron X-ray fluorescence and W L_3 -edge absorption spectra were measured from the sample at temperatures up to 873 K and at pressures up to 200 MPa on the undulator PNC/XSD ID20 beamline of the Advanced Photon Source. The incident X-ray beam flux was approximately 1×10^{11} photons s⁻¹. A seven-element Li-drifted Ge Canberra detector was placed horizontally at 90° orientation to the incident micro-focused (~ 4 μ m diameter) X-ray beam. The flux density at the sample position was about 8×10^9 photons μm^{-2} s⁻¹ and the dose volume in the

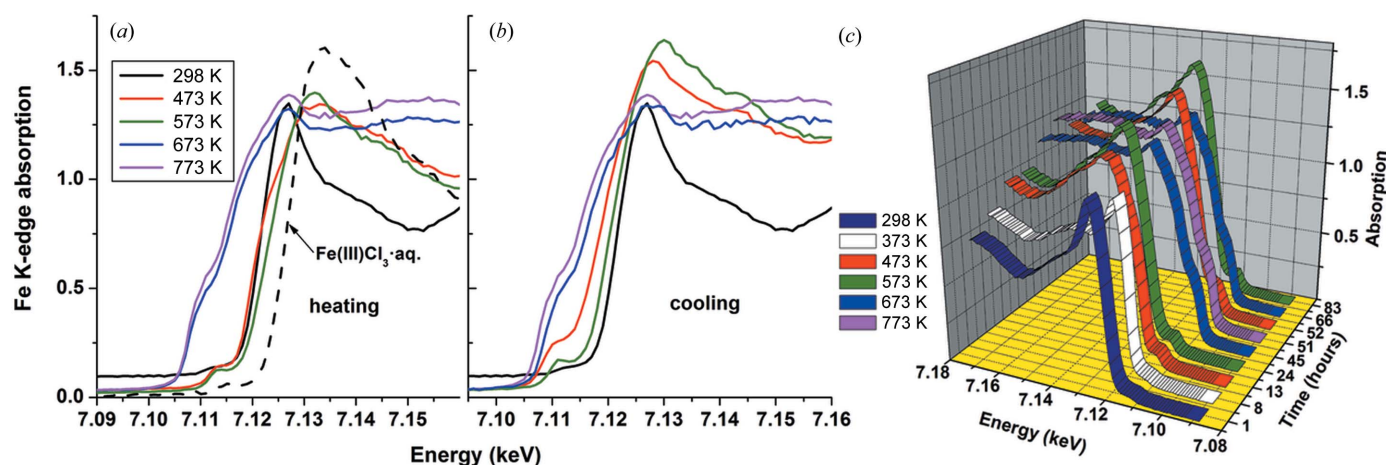


Figure 1

Fe K -edge XANES data measured from a 0.1 M Fe(II)Cl₂ aqueous solution sample, upon (a) heating and (b) cooling, using a bending-magnet beamline of the Cornell High Energy Synchrotron Source (CHESS). The thermal history of the sample is illustrated in (c); the XANES measured from a 0.1 M Fe(III)Cl₃ aqueous solution sample at 298 K (dashed line) is shown in (a) for comparison. The Fe(II)Cl₂ aqueous solution sample was exposed discontinuously to synchrotron radiation for approximately half of the 87 h duration of the experiment (Anderson *et al.*, 2012).

sample was approximately $3.3 \times 10^3 \mu\text{m}^3$. Incident X-ray beam harmonics were reduced by 15% detuning of the Si(111) monochromator crystals from the incident X-ray flux intensity maximum. The sample in the HDAC was viewed using a video camera mounted on a microscope equipped with a long-working-distance 10× Mitutoyo objective lens.

4.2. Fe(II)Cl₂ aqueous solutions

4.2.1. Samples and cell loading. Two iron(II) chloride [0.34 and 0.69 M Fe(II)Cl₂] aqueous solutions were prepared in argon atmosphere using 99.99% pure ferrous chloride anhydrous powder (Alfa Aesar) and de-oxygenated deionized water. Transfer of each solution into the HDAC was performed in a glove bag that was purged with argon gas. The lower diamond anvil has milled grooves on opposite sides of the recess for enhanced transmission of X-rays. Fig. 2 (inset) shows a scanning electron microscopy image of the sample recess, measuring 200 μm × 300 μm across and 50 μm in depth, milled using focused ion beam (FIB) into the face of a diamond anvil. As with the WO₃ + H₂O sample, the Fe(II)Cl₂ fluid sample was sealed between the diamond anvils without the use of a gasket. The sample pressures, estimated from the equation of state of the fluid and procedures outlined above, ranged from atmospheric at room temperature to 40 MPa at 773 K. The 0.34 M Fe(II)Cl₂ aqueous sample was placed in a sample recess with a path length of 300 μm, so that its XAS step height was approximately the same as that of the 0.69 M Fe(II)Cl₂ aqueous sample loaded in an HDAC with a 200 μm sample path length. This sample yielded almost identical data to that of the 0.69 M Fe(II)Cl₂ aqueous sample. The samples were equilibrated for at least 15 min at each *P*–*T* point, prior to exposure to the X-ray beam. Additional operational and

design details concerning the HDAC have been given elsewhere (Bassett *et al.*, 2000b; Mayanovic *et al.*, 2007a).

4.2.2. Data collection. *In situ* ED-XAS measurements were made on the Fe(II)Cl₂ aqueous samples at the Fe *K*-edge on beamline ID24 at the European Synchrotron Research Facility (ESRF) (Pascarelli *et al.*, 2006). The energy scale for the ED-XAS data was calibrated by comparing data acquired on pure iron foil using the energy-dispersive spectrometer on ID24 and a standard energy scanning beamline (BM29 at the ESRF). The X-ray beam was focused to ~5 μm × 15 μm FWHM (horizontal × vertical) at the sample position. Up to 100 ED-XAS spectra were measured in transmission mode from the Fe(II)Cl₂ aqueous samples at photon energies ranging approximately from 7.07 to 7.29 keV. Each ED-XAS spectrum used in the analysis is an accumulation of up to 100 individual absorption spectra; each accumulation was measured for 10 ms. The ED-XAS spectra were first measured in short and subsequently in long time-resolution sequences, at each temperature point. The short sequence consists of 100 ED-XAS spectra measured with 1 s time resolution whereas the long sequence consists of 30 or 60 spectra measured at 60 s time resolution. The incident flux was ~1 × 10¹³ photons s⁻¹ over the full energy range of the diffracted polychromatic fan. The flux density at the sample was ~2 × 10¹¹ photons μm⁻² s⁻¹ and the sample dose volume was about 1.2 × 10⁴ μm³. Aluminium sheets (~0.41 mm thickness) were placed in front of the sample to attenuate the beam during alignment, in order to minimize the radiolysis process before the ED-XAS measurements. Complete details on the operation of beamline ID24 at ESRF have been discussed by Pascarelli *et al.* (2006).

4.2.3. Data analysis. The X-ray absorption near-edge structure (XANES) data (Fig. 3) clearly show a continuous overall shift in X-ray energy with irradiation time; in parti-



Figure 2 The HDAC shown in the experimental set-up at beamline ID24 at ESRF, that was used to make ED-XAS measurements of Fe(II)Cl₂ aqueous solution samples to 773 K. The inset shows a scanning electron microscopy image of the 200 μm × 300 μm × 50 μm (depth) sample recess milled with focused ion beam into the face of a diamond anvil of the HDAC.

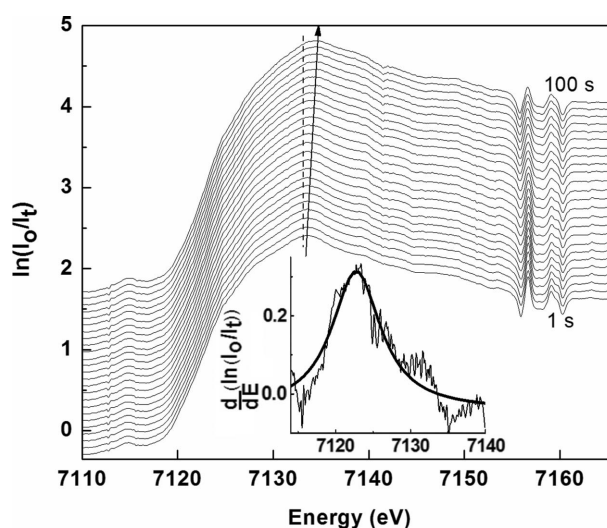


Figure 3 ED-XANES data clearly exhibiting a continuous overall positive shift in energy with irradiation time ranging from 1 to 100 s, measured from a 0.69 M Fe(II)Cl₂ aqueous solution sample at 573 K. The inset shows a Lorentzian peak (thick smooth line) fitted to the derivative of the ED-XANES (thin irregular line) measured at 1 s that is used to determine the location of the Fe *K*-edge.

cular, the arrow indicates a shift toward higher energies of the maximum of the absorption at ~ 7134 eV. The data were first differentiated, by averaging the slope of two adjacent data points, in the XANES region, from approximately 7110 to 7150 eV. The differentiated data were subsequently fit using the Lorentzian peak shape *via* automated routines developed within the *Origin 7* (OriginLab) analysis software. The centroid value of each Lorentzian peak fitted to the derivative data was used to determine the Fe *K*-edge energy (E_0) value of the ED-XAS spectrum. The inset of Fig. 3 shows a Lorentzian peak fitted to the derivative of a typical ED-XAS spectrum in the XANES region. The analysis of the edge-energy drift of the small pre-edge peak occurring at approximately 7115 eV in the XANES was found to be substantially less accurate than use of the first derivative of the spectra and was therefore not used in the overall analysis. In addition to the procedures described above, the linear combination fit (LCF) in *Athena 0.8* software was used on the ED-XAS spectra in the XANES region (-20 to 30 eV) to ascertain the Fe *K*-edge energy drift as a function of time (Ravel & Newville, 2005). Whereas LCF produced results in reasonably good agreement, the method is nevertheless noticeably less accurate in comparison with the analysis of the differentiated XAS data described above. The most obvious advantage of our analysis method in comparison with LCF is that our method does not require normalization of the XAS spectra. The drifts in E_0 that we measure are very small, but they are clearly detectable because the enhanced stability of the ED-XAS optics (*i.e.* no moving component during acquisition, contrary to the energy scanning spectrometers) enables reduction in the sources of non-statistical noise, leading to higher precision on reproducibility of the energy scale.

The time-resolved E_0 data were fit most accurately using non-linear least squares and a second-order exponential decay function of the general form

$$E_0 = E_0^f + A_1 \exp(-k_1 t) + A_2 \exp(-k_2 t). \quad (1)$$

In (1), E_0 is the time-dependent edge energy value and E_0^f is the edge energy as $t \rightarrow \infty$. The A_1 and A_2 parameters are energy kinetic rate coefficients, and k_1 and k_2 are time rate constants. The use of (1) is appropriate because the natural log plot of the data clearly exhibits two distinct linear slopes, indicative of two separate kinetic processes (see Fig. 5).

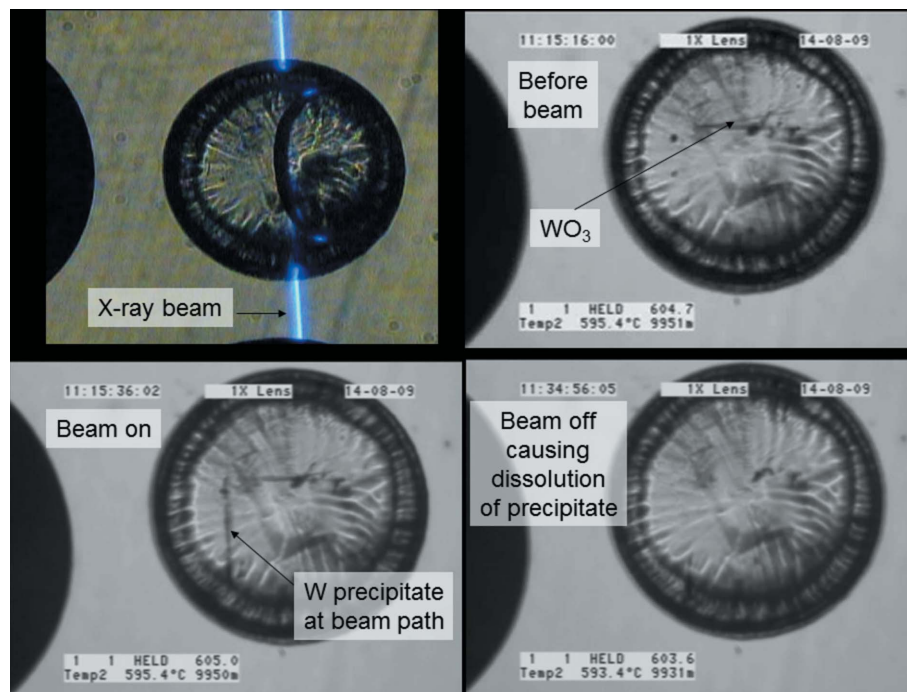


Figure 4

The upper left panel shows the visible fluorescence from the focused X-ray micro-beam as it traverses through the sample recess of the diamond anvil in the hydrothermal diamond anvil cell (HDAC). The remaining panels show a sequence of images captured from a video recording of the $\text{WO}_3 + \text{H}_2\text{O}$ sample in the HDAC at 873 K. The upper right panel shows the sample at 11:15:16 before exposure to the X-ray beam. With the X-ray beam turned on, a dark colloidal precipitate streak is clearly visible at the bottom of the recess at 11:15:36 in the lower left panel. The lower right panel shows that the previously formed precipitate has dissolved into the supercritical fluid, after the X-ray beam is turned off.

5. Results and discussion

5.1. $\text{WO}_3 + \text{H}_2\text{O}$ system at high P - T conditions

The WO_3 and water sample was heated to 873 K and equilibrated at this temperature for over an hour without any exposure to X-rays. At this temperature the WO_3 crystal was almost entirely dissolved. At the moment when the sample was exposed to the X-ray beam, a dark precipitate formed along the focused beam path through the fluid. Fig. 4 shows a sequence of images captured from a video recording of the experiment. The video clip is provided in the supplementary information.¹ As the time stamp on the video shows, there is no dark precipitate streak in the sample recess before exposure to the X-ray beam at 11:15:16. The dark precipitate streak is clearly visible at the bottom of the recess at 11:15:36. Note that the precipitate streak is only formed at the beam path and nowhere else in the sample. At this point the sample is no longer exposed to the X-ray beam and the black precipitate begins to dissolve into the supercritical fluid. By 11:34:56 (the lower right panel of Fig. 4) the precipitate is completely dissolved into the fluid phase. The procedure shown in Fig. 4 was repeated multiple times showing the reversibility and reproducibility of the effect (*i.e.* formation of the precipitate

¹ Supplementary data for this paper are available from the IUCr electronic archives (Reference: HF5204). Services for accessing these data are described at the back of the journal.

when the X-ray beam is turned on and dissolution of the precipitate back into the fluid with the beam turned off). Clearly, the formation of the precipitate is caused by the X-ray radiolysis-induced effects on aqueous tungsten species and is not due to chemical effects exhibited by the sample under supercritical conditions. Similar X-ray beam radiolysis-induced precipitate formation was observed with Fe(II) (§3 of this paper), Cu(II) (Jayanetti *et al.*, 2001), Yb(III) (Mayanovic *et al.*, 2002) and Gd(III) (Mayanovic *et al.*, 2007*b*) chloride and Gd(III) nitrate aqueous solutions under high P - T conditions. Mesu *et al.* (2006) have recently documented synchrotron X-ray radiolysis-induced formation of copper colloidal precipitate in chloride-bearing aqueous solutions. In the case of aqueous copper chloride solutions, we determined that radiolysis-induced reduction of Cu^{2+} to Cu^0 led to formation of native copper clusters and nanoparticles. Complete characterization of the beam-induced precipitate produced in the present experiment is currently in progress.

5.2. Fe(II)Cl₂ aqueous solutions from 573 to 773 K

Fig. 5 shows a plot of E_0 as a function of time, and the fitted curve to these values, for data measured from the 0.69 M Fe(II)Cl₂ aqueous sample at 573 K. As can be seen from Fig. 5, the E_0 values of the iron chloride aqueous sample increase exponentially with time. These data indicate that a significant percentage of the Fe^{2+} ions in solution undergo oxidation due to reaction with radiolysis products within 100 s of exposure to synchrotron radiation at 573 K. It should be emphasized that the initial E_0 value shown in Fig. 5 is shifted with respect to the edge energy value of aqueous Fe^{2+} species in iron(II) chloride solutions because the sample was previously exposed intermittently to synchrotron radiation for at least 8.7 min, for sample alignment and test runs, and had therefore undergone

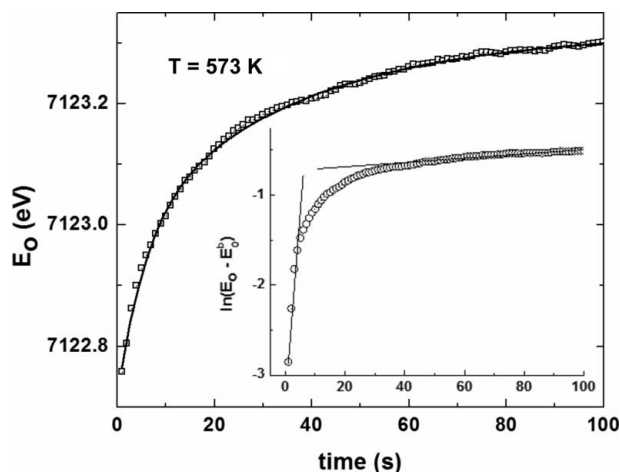


Figure 5 Fe K -edge energy (E_0) values, shown as square points, as a function of time to 100 s, measured from a 0.69 M Fe(II)Cl₂ aqueous solution sample at 573 K. The average error in E_0 is ± 0.08 eV, as determined from Lorentzian peak fitting. The solid line is the fit to the data using a second-order exponential decay function [equation (1)]. The inset shows a natural log plot of the quantity $(E_0 - E_0^b)$, where E_0^b is an estimated edge energy value of 7122.7 eV at $t = 0$, clearly exhibiting two distinct linear slopes indicative of two separate kinetic processes. The straight lines are guides to the eye only.

some degree of radiolysis. Figs. 6 and 7 show plots of E_0 values versus time for data measured from the 0.69 M Fe(II)Cl₂ aqueous sample at 673 and 773 K, respectively. Fig. 6 shows data for measurements to 100 s at 1 s time resolution whereas Fig. 7 data range to 1800 s at 60 s resolution. The lines in Figs. 5–7 are the fitted curves to the E_0 data. An aberrant data point occurring at ~ 1500 s in Fig. 7 was excluded from the fitted data set. The data shown in Fig. 6 indicate reduction of a significant percentage of the Fe^{3+} aqueous species owing to reaction with radiolysis products within 100 s of exposure to synchrotron radiation at 673 K. Similarly, data shown in Fig. 7 indicate reduction of Fe^{3+} and Fe^{2+} aqueous species owing to X-ray-induced radiolysis effects at 773 K. Evidence from E_0 data measured at 773 K, and from our previous experiments (see Fig. 1) made on the Fe(II)Cl₂ aqueous system, indicate that Fe^{2+} species are radiolytically reduced to Fe^0 in aqueous solutions after exposure to synchrotron X-rays (*i.e.* the reduction reaction progression is $\text{Fe}^{3+} \rightarrow \text{Fe}^{2+} \rightarrow \text{Fe}^0$).

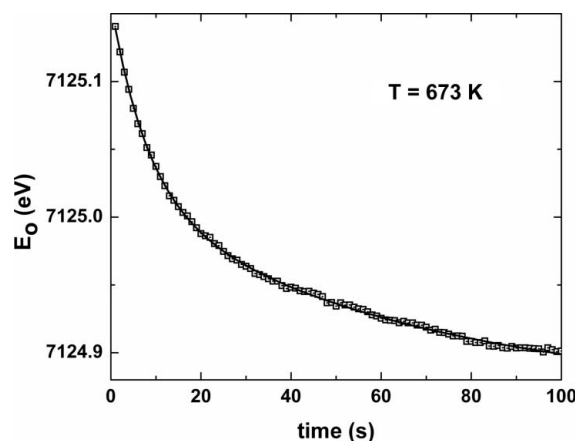


Figure 6 Fe K -edge energy (E_0) values, shown as square points, as a function of time to 100 s, measured from a 0.69 M Fe(II)Cl₂ aqueous solution sample at 673 K. The solid line is the fit to the data. The average error in E_0 is ± 0.13 eV, as determined from Lorentzian peak fitting.

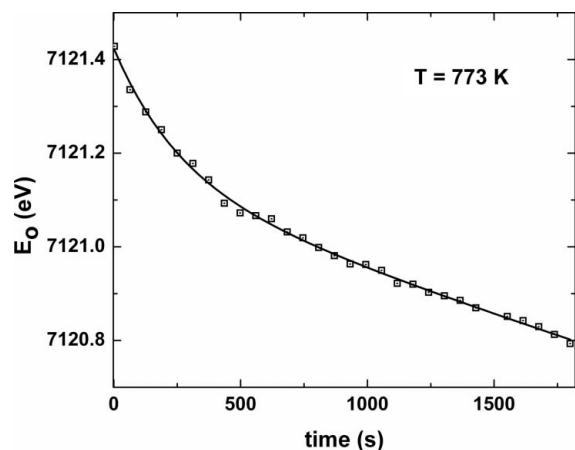


Figure 7 Fe K -edge energy (E_0) values (squares) as a function of time to 1800 s, measured from a 0.69 M Fe(II)Cl₂ aqueous solution sample at 773 K and at 60 s intervals. The solid line is the fit to the data. An aberrant data point occurring at ~ 1500 s was excluded from the data set. The average error in E_0 is ± 0.09 eV, as determined from Lorentzian peak fitting.

Table 1

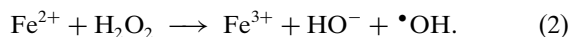
Results obtained from fitting the 1 s time-resolved E_0 data using the general form of equation (1).

A_1 and A_2 are the energy kinetic rate coefficients and k'_1 and k'_2 are the time rate constants. The estimated errors shown are at the 1σ confidence level.

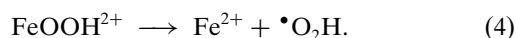
T (K)	k'_1 (s^{-1})	k'_2 (s^{-1})	A_1 (eV)	A_2 (eV)
573	0.029 ± 0.001	0.18 ± 0.01	-0.331 ± 0.008	-0.277 ± 0.009
673	0.015 ± 0.001	0.123 ± 0.004	0.148 ± 0.002	0.142 ± 0.003
773	0.008 ± 0.242	0.4 ± 2.0	0.2 ± 3.8	0.01 ± 0.02

The results from fitting of the time-resolved data (at 1 s resolution) are shown in Table 1. The k'_1 and k'_2 time rate constants, in units of s^{-1} , are directly related to the pseudo first rate time constant k from the rate equation $r = k[Fe^{n+}][B] = k'[Fe^{n+}]$, where n is 2 or 3 and $[B]$ is the concentration of a radiolytic species causing oxidation of ferrous or reduction of ferric and ferrous species. Examples of radiolytic species B include H_2O_2 , $\bullet OH$, H_2^+ , $\bullet O_2H$, O_2^- and e_{aq}^- . The nature of our experiment precludes the measurement of $[B]$ and, therefore, exact determination of the pseudo first rate time constant k . Based on estimates of the yields of radiolytic species in water owing to high-energy X-rays (Ferradini & Jay-Gerin, 2000) and effective X-ray dose in the sample (accounting for loss of X-ray photon flux owing to transmission through air and diamond), we estimate that the concentration of radiolytic species B ranges from approximately 0.001 to 0.01 M under ambient conditions.

At this time we can only speculate on the nature of the synchrotron X-ray-induced radiolytic reaction that is responsible for oxidation of Fe^{2+} species in the aqueous fluid at 573 K. A Fenton-type reaction with the radiolysis product H_2O_2 can cause oxidation of the Fe^{2+} ion according to the following equation,



The rate constant value for the Fenton-type reaction (2) is $52 M^{-1} s^{-1}$ at room temperature increasing by up to three orders of magnitude at 573 K (Takagi & Ishigure, 1985). Using the estimated values for $[B]$ from above and taking into account thermal decomposition of radiolytic products such as H_2O_2 under elevated temperature conditions (Takagi & Ishigure, 1985; Štefanić & LaVerne, 2002; Lee & Yoon, 2004), our estimate for the k_2 rate constant (*i.e.* $k_2 = k'_2/[B]$) ranges roughly from 0.2 to $2 \times 10^3 M^{-1} s^{-1}$ at 573 K. Similarly, a slow reduction reaction of Fe^{3+} occurs upon reaction with H_2O_2 according to the two-step reaction



The upper limit of the $Fe^{3+}-\bullet O_2H$ reaction in room-temperature aqueous solutions has been determined to be $10^3 M^{-1} s^{-1}$ (Rush & Bielski, 1985; Perez-Benito, 2004). Using the same estimates as given above, we calculate k_2 rate constant values of approximately 2×10^3 and $1 \times 10^4 M^{-1} s^{-1}$ at 673 and 773 K, respectively. Taking into account the fact that rates of

reactions in aqueous solutions increase with temperature owing to enhanced diffusion, our estimated values for the k_2 rate constant appear to be in order-of-magnitude agreement with the previously determined limiting values for the $Fe^{3+}-\bullet O_2H$ reaction. Based on these comparisons, we speculate that the synchrotron X-ray-induced radiolytic Fenton-type reaction (2) may contribute to the oxidation of Fe^{2+} species at 573 K, and that the two-step reaction (3) and (4) may contribute to the reduction of iron species in the $FeCl_2$ -water system at 673 to 773 K. In addition, it is conceivable that the mechanisms responsible for the reduction or oxidation of iron species include intermediate reactions between primary radiolysis products and the chloride ligand under high P - T aqueous solutions. A recent study (Mesu *et al.*, 2006) showed that ligand type can have a determinative effect on the rate of reduction of Cu^{2+} ions owing to X-ray-induced radiolysis effects in room-temperature aqueous solutions. In our future experiments, *in situ* Raman spectroscopy used simultaneously with ED-XAS of $FeCl_2$ -aqueous samples may prove beneficial for detection of radiolytic species (B) and revealing the nature of the reactions responsible for the oxidation and reduction of iron species under high P - T conditions. The k'_1 rate constant is indicative of a competing complementary process, with slower kinetics than the oxidation or reduction reactions associated with the k'_2 rate constant. The source of the mechanism responsible for the processes reflected by this rate constant is unknown. It is unlikely that the k'_1 rate constant reflects a diffusion-limited process because of its apparent reduction with increasing temperature.

The oxidation-reduction effect due to radiolysis was found to be partially reversible upon cooling of the aqueous samples from 773 to 573 K, without irradiation by X-rays. Irradiation of the sample with X-rays at 573 K upon cooling gave almost identical rate constant results as upon heating. Data collected at 60 s resolution from the samples held at 573 or 673 K confirmed the results described above. However, analysis of ED-XAS data collected at 60 s resolution from the 0.69 M $Fe(II)Cl_2$ aqueous sample held at 773 K (see Fig. 7) gave kinetic rate constant results that were three to five orders of magnitude smaller than k'_2 measured at 1 s resolution. Although the processes responsible for the slow kinetics observed from the $Fe(II)Cl_2$ aqueous sample at 773 K at 60 s resolution are unknown, the reduction of Fe^{2+} species and sample relaxation mechanisms may play a role under these conditions.

Our results show that a significant proportion of the iron species are either oxidized or reduced, depending upon the P - T conditions of the aqueous fluid, within a short period of time (100 s) owing to synchrotron X-ray-induced radiolysis effects. These effects become more pronounced with extended exposure time of the aqueous solution sample in the synchrotron X-ray beam. In addition, we find that aqueous tungsten ions form a colloidal precipitate soon after exposure to a synchrotron X-ray micro-beam in a $WO_3 + H_2O$ system at 873 K and 200 MPa as a result of radiolysis-induced effects. Accordingly, investigations of structural and chemical properties (*e.g.* speciation) of iron and tungsten ions in high P - T

aqueous solutions using synchrotron X-ray radiation may require special precautions. The structural and chemical properties of aqueous metal ions are principally affected by the solution P - T conditions, pH, solute concentrations and gas (O_2 , H_2 etc.) fugacities. However, reactions owing to X-ray-radiolysis may result in significant modifications in the chemistry of aqueous solutions and, accordingly, to substantial changes in speciation and structure properties of aqueous metal ions. Such concerns are relevant to synchrotron X-ray studies of other multivalent metal ions, such as Cu^{2+} , Cr^{3+} , Mn^{2+} and Ni^{2+} , in aqueous solutions to high P - T conditions.

In terms of applications, our results show that, despite the potential formation of tungsten oxides such as WO_3 , radiolysis-induced effects may cause colloidal precipitate formation from tungsten ions in the reactor vessel high P - T aqueous fluids of supercritical-water-cooled nuclear reactors. Similarly, iron species may become either oxidized, reduced or may form a precipitate, depending upon the P - T and radiation conditions of the aqueous fluid in the nuclear reactor vessel. Precipitate formation resulting from radiolysis could potentially have a beneficial aspect because the concentration of metal ions in solution would effectively be lowered thereby reducing the corrosive potential of supercritical aqueous fluids within the primary cooling loops of nuclear reactors. Our studies suggest that H_2O_2 may be an important radiolysis product that reacts with iron species in aqueous fluids at near to supercritical conditions. Because the LET is greater for fast neutron recoil protons than for X-rays in the energy region of this study, the implication is that H_2O_2 may play an important role in causing radiolysis-induced effects on aqueous iron species under supercritical conditions in water-cooled nuclear reactors. Further studies are required to fully understand radiolysis effects due to ionizing radiation on metal ions in aqueous fluids to supercritical conditions.

We acknowledge the European Synchrotron Radiation Facility for provision of research beam time. We thank Florian Perrin and others at the ID24 beamline and for experimental assistance at the ESRF, Dave Mao for kindly granting us partial use of his general user beam time on the beamline and Richard Wirth for FIB milling of diamonds. RAM and HAND were supported as part of the EFree, an Energy Frontier Research Center funded by the US Department of Energy, Office of Science, Office of Basic Energy Sciences under award No. DE-SC0001057. AJA acknowledges support from NSERC and Natural Resources Canada's (NRCAN) Office of Energy Research and Development and Atomic Energy of Canada Limited (AECL). The Pacific Northwest Consortium X-ray Science Division PNC/XSD facilities are supported by the US Department of Energy, Basic Energy Sciences, a Major Resources Support grant from NSERC, the University of Washington, the Canadian Light Source and the Advanced Photon Source. Use of the Advanced Photon Source, an Office of Science User Facility operated for the US Department of Energy (DOE) Office of Science by Argonne National

Laboratory, was supported by the US DOE under contract No. DE-AC02-06CH11357.

References

- Anderson, A. J., Mayanovic, R. A., Bassett, W. A. & Chou, I.-M. (2012). In preparation.
- Bassett, W. A., Anderson, A. J., Mayanovic, R. A. & Chou, I.-M. (2000a). *Chem. Geol.* **167**, 3–10.
- Bassett, W. A., Anderson, A. J., Mayanovic, R. A. & Chou, I.-M. (2000b). *Z. Kristallogr.* **215**, 711–717.
- Bouchard, J. (2009). *Proceedings of the GIF Symposium*, Paris, France, *The Generation IV International Forum (GIF) Symposium*, pp. 11–13 (<http://www.Gen-4.Org/GIF/About/ProceedingsofGIFSymposium.htm>).
- Boyle, K. P., Brady, D., Guzonas, D., Khartabil, H., Leung, L., Lo, J., Quinn, S., Suppiah, S. & Zheng, W. (2009). *Proceedings of the 4th International Symposium on Supercritical Water-Cooled Reactors*, Heidelberg, Germany, paper No. 74 (<http://www.hplwr.eu/public/symposium.html>).
- Buxton, G. V. (1987). *Radiation Chemistry Principles and Applications*, edited by Farhataziz and M. A. J. Rodgers, p. 321. New York: VCH.
- Chou, I.-M., Anderson, A. J., Bassett, W. A., Mayanovic, R. A. & Shang, L. (2008). *Rev. Sci. Instrum.* **79**, 115103.
- Christensen, H. (2006). *Fundamental Aspects of Water Coolant Radiolysis*. SKI Report 2006:16. Stockholm: Swedish Nuclear Power Inspectorate.
- Christensen, H. & Sehested, K. (1981). *Radiat. Phys. Chem.* **18**, 723–731.
- Draganic, I. G. & Draganic, Z. D. (1971). *The Radiation Chemistry of Water*. New York: Academic Press.
- Elliot, A. J. (1994). *Rate Constants and G-Values for the Simulation of the Radiolysis of Light Water over the Range 0–300 °C*. Chalk River: Atomic Energy of Canada.
- Elliot, A. J., Ouellette, D. C. & Stuart, C. R. (1996). *The Temperature Dependence of the Rate Constants and Yields for the Simulation of the Radiolysis of Heavy Water*. Chalk River: Atomic Energy of Canada.
- Ferradini, G. & Jay-Gerin, J.-P. (2000). *Res. Chem. Intermed.* **26**, 549–565.
- Garrett, B. C. et al. (2005). *Chem. Rev.* **105**, 355–390.
- Guzonas, D., Tremaine, P. & Brosseau, F. (2009). *Proceedings of the 4th International Symposium on Supercritical Water-Cooled Reactors*. Heidelberg, Germany, paper No. 67 (<http://www.hplwr.eu/public/symposium.html>).
- Hoel, A., Reyes, L. F., Heszler, P., Lantto, V. & Granqvist, C. G. (2004). *Curr. Appl. Phys.* **4**, 547–553.
- Hoffmann, M. M., Darab, J. G., Heald, S. M., Yonker, C. R. & Fulton, J. L. (2000). *Chem. Geol.* **167**, 89–103.
- Ihli, T., Basub, T. K., Giancarli, L. M., Konishid, S., Malange, S., Najmabadif, F., Nishiog, S., Raffray, A. R., Raoh, C. V. S., Sagarai, A. & Wu, Y. (2008). *Fusion Eng. Des.* **83**, 912–919.
- Jayanetti, S., Mayanovic, R. A., Anderson, A. J., Bassett, W. A. & Chou, I.-M. (2001). *J. Chem. Phys.* **115**, 954–962.
- Klueh, R. L. (2004). Report ORNL/TM-2004/176. Oak Ridge National Laboratory, TN, USA.
- Kritzer, P. (2004). *J. Supercrit. Fluids*, **29**, 1–29.
- LaVerne, J. A. & Pimblott, S. A. (1993). *J. Phys. Chem.* **97**, 3291–3297.
- Lee, C. & Yoon, J. (2004). *Chemosphere*, **56**, 923–934.
- Lundström, T., Christensen, H. & Sehested, K. (2004). *Radiat. Phys. Chem.* **69**, 211–216.
- McCracken, D. R., Tsang, K. T. & Laughton, P. J. (1998). *Aspects of the Physics and Chemistry of Water Radiolysis by Fast Neutrons and Fast Electrons in Nuclear Reactors*. Chalk River: Atomic Energy of Canada.
- Matthews, R. W. (1982). *Intl. J. Appl. Radiat. Isot.* **33**, 1159–1170.

- Mayanovic, R. A., Anderson, A. J., Bassett, W. A. & Chou, I.-M. (2007a). *Rev. Sci. Instrum.* **78**, 053904.
- Mayanovic, R. A., Anderson, A. J., Bassett, W. A. & Chou, I.-M. (2007b). *Chem. Geol.* **239**, 266–283.
- Mayanovic, R. A., Anderson, A. J., Bassett, W. A., Chou, I.-M. & Shea-McCarthy, G. (1999). National Synchrotron Light Source Activity Report 1998. NSLS, Brookhaven, NY, USA.
- Mayanovic, R. A., Jayanetti, S., Anderson, A. J., Bassett, W. A. & Chou, I.-M. (2002). *J. Phys. Chem. A*, **106**, 6591–6599.
- Mesu, J. G., Beale, A. M., de Groot, F. M. & Weckhuysen, B. M. (2006). *J. Phys. Chem. B*, **110**, 17671–17677.
- Neeb, K. H. (1997). *The Radiochemistry of Nuclear Power Plants with Light Water Reactors*. Berlin: Walter de Gruyter.
- Pascarelli, S., Mathon, O., Muñoz, M., Mairs, T. & Susini, J. (2006). *J. Synchrotron Rad.* **13**, 351–358.
- Perez-Benito, J. F. (2004). *J. Phys. Chem. A*, **108**, 4853–4858.
- Ravel, B. & Newville, M. (2005). *J. Synchrotron Rad.* **12**, 537–541.
- Rush, J. D. & Bielski, B. H. J. (1985). *J. Phys. Chem.* **89**, 5062–5066.
- Shaw, R. W., Thomas, B. B., Antony, A. C., Charles, A. E. & Franck, E. U. (1991). *Chem. Eng. News*, **69**, 26–39.
- Spinks, J. W. T. & Woods, R. J. (1990). *An Introduction to Radiation Chemistry*, 3rd ed. New York: Wiley-Interscience.
- Štefanić, I. & LaVerne, J. A. (2002). *J. Phys. Chem.* **106**, 447–452.
- Takagi, J. & Ishigure, K. (1985). *Nucl. Sci. Eng.* **89**, 177–186.
- Wagner, W. & Pruss, A. (2002). *J. Phys. Chem. Ref. Data*, **31**, 387–535.